Asian Journal of Chemistry; Vol. 33, No. 10 (2021), 2446-2454

ASIAN JOURNAL OF CHEMISTRY

https://doi.org/10.14233/ajchem.2021.23403

Synthesis, Optical, Photocatalytic and Electrochemical Properties of Cobalt Doped ZnS Nanoparticles

K.R. Sumadevi[1], G. Krishnamurthy[1,*], H.S. Bhojya Naik[2], Prabhaker Walmik[1], Malathesh Pari[1], N. Ranjitha[1], R.S. Priya Rani[3] and P. Parameshwara Naik[1]

[1]Department of P.G. Studies and Research in Chemistry, Sahyadri Science College (A Constituent College of Kuvempu University), Shivamogga-577203, India
[2]Department of Studies and Research in Industrial Chemistry, School of Chemical Sciences, Kuvempu University, Shankaraghatta-577451, India
[3]Department of Studies and Research in Chemistry, School of Chemical Sciences, Kuvempu University, Shankaraghatta-577451, India

*Corresponding author: E-mail: gkmnaiksahyadri@gmail.com

Received: 7 July 2021; *Accepted*: 9 August 2021; *Published online*: 20 September 2021; AJC-20519

Poly(vinyl pyrrolidone) capped and uncapped Co:ZnS nanoparticles have been synthesized by co-precipitation method. These synthesized nanoparticles were characterized using spectral techniques and the optical and photoluminescence properties of nanoparticles were also studied. Poly(vinyl pyrrolidone) capped nanoparticles has been studied for the electrochemical sensing of various biomolecules. The Co:ZnS modified glassy carbon electrode (GCE) proved to be effective nanoparticles composite electrode to detect biomolecules electrochemically with a wide linear detection range of 0.2 to 1.6 µmol/L, Also a low detection limit (LOD) of 0.06 µM/L and excellent sensitivity of 4.366 µA μM^{-1} has been obtained. It is observed that the particle size of nanoparticles is affected by the capping agent. It is therefore the modified electrode has become a good electrode material with a greater stability without leaching. The optical band gap was determined by UV-visible spectra and the value is found to be in the range of 3.75 to 4.00 eV. The photocatlytic activity on Eriochrome black T dye in the visible region using nanoparticles has been determined. It was found that the capped nanoparticles are more effective in photocatalytic degradation due to low energy consumption and safe recovery of it after catalytic performance from polluted water.

Keywords: Co-doped ZnS nanoparticles, Eriochrome Black-T, Dopamine, Uric acid, Sensors.

INTRODUCTION

In the past decade, studies on particles with small size have received attention. The thermal, optical and mechanical properties of nanoparticles are different from those of their bulk counterparts [1,2]. Additionally, nanosize particles exhibit excellent electrochemical and catalytic properties [3,4]. For stained water, dye degradation is the standard method employed to determine the photocatalytic activity of photocatalysts, including energy consumption and safety. Thus, nanoparticles present potential applications in various commercial fields, such as wastewater treatment plants, paint industry, refrigerator coatings, electrical industry and detergents, *etc*. [5-7]. The physico-chemical properties, such as small size and optical properties, of the nanoparticles of zinc oxide render them promising candidates for different medical applications [8-10]. These applications include imaging and drug delivery techniques. In various commercial sectors, ZnS nanoparticles most frequently employed. The energy of a wide bandgap increases the photocatalytic activity. The catalytic properties are used in industries, such as waste water treatment plants, cosmetics, paint and textile industries [11,12]. Through the exchange of holes and electrons in particles, light absorption by ZnS nanoparticles causes reactive oxygen species formation [13,14]. Radicals can degrade or destroy the organic matter, hence, can result in the ecological disturbance [15]. Photocatalytic activities chiefly rely on surface properties, including particle size, shape and morphology [16,17]. Modifying surface properties can change the particle photocatalytic efficiency. Different approaches involving capping with inorganic and organic compounds and doping using transition metals are employed to improve the photocatalytic characteristics of nano-

particles [18,19]. Additionally, capping materials can lead to a decrease in particle dissolution, thereby further alleviating the toxicity risk [20].

Among the semiconductors of II-VI groups, ZnS is non-toxic and has a wide bandgap. Thus, ZnS is an excellent host for many rare earth and transition metal ion dopants. ZnS produces outstanding photocatalytic and optical properties. The ZnS nanoparticle bandgap is 3.37 eV. Thus, ZnS nanoparticles can absorb the light that exceeds or is within this bandgap energy. Since ZnS nanosemiconductors doped with Mn^{2+} were reported to provide life-time reduction and high luminescence efficiency, the doped nanocrystals of ZnS have received considerable attention [21]. The doped nano-semiconductors generate a novel class of the luminescent material and present various lighting, display, and sensor applications [22]. Different studies [23-27] reported the photocatalytic and optical properties of ZnS nanocrystals doped with various transition metal ions. ZnS nanoparticles doped with Co are ideal for exploring electrochemical properties. Literature has reported the magnetic and luminescent properties of ZnO nanoparticles doped with Co and different results including quenching and luminescence development. The capping agent must be bonded to nanoparticles to enhance the surface states, which affect nanoparticle optoelectronic properties and to minimize larger particle formation [28]. ZnS capped with poly(vinyl pyrrolidone) nanoparticles exhibits improved luminescence properties compared with that capped with other agents.

ZnS nanoparticle with different structure and morphology were studied using a variety of methods. Among all these, the preparation of ZnS nanoparticles *via* chemical co-precipitation method assisted route with poly(vinyl pyrrolidone) (PVP) acquire a agreat attention because it provides a favourable factors such as large scale production, high yield and this synthesis method has a great influence on their size, shape and also reduces the cost of production. Hence, PVP has been chosen as a stabilizer in the present work. In this present work, the effect of cobalt doping on the structural, optical and photocatalytic properties of PVP capped and uncapped nanoparticles were studied. The synthesized ZnS doped nanoparticles used to evaluate its electrochemical sensing property of various biomolecus. The synthesized nanoparticles modified glassy carbon electrode (GCE) proved to be a very effective electrode material to detect biomolecules electrochemically with a wider linear detection.

EXPERIMENTAL

Nanosized particles of ZnS crystals were prepared by chemical co-precipitation reaction using analytical reagent grade chemicals analytical grade zinc acetate dehydrate $Zn(CH_3COO)_2 \cdot 2H_2O$, cobaltaous acetate $Co(CH_3COO)_2 \cdot 2H_2O$, sodium sulfide ($Na_2S \cdot xH_2O$), poly(vinyl pyrrolidone) (PVP) and dopamine were purchased from Loba chemie, Nice Chemicals and Merck chemicals, respectively. Deionized water was used throughout for the preparation process.

The synthesized naoparticles were characterized using powder XRD Rigaku MiniFlux 650, FTIR Thermo fisher-i55, UV-Visible spectrophotometer-119 while the morphological studies carried out by SEM and EDX techniques. Cyclic voltammetric (CV) measurements were carried out using CHI620E with latest windows based acquisition s/w at ambient temperature. Three electrode systems was used for electrochemical study using GCE as a working electrode (area 0.05 cm^2), saturated Ag/AgCl (saturated KCl) as a reference electrode and Pt wire as a counter electrode.

Synthesis: Semiconducting nanoparticles of PVP capped ZnS and cobalt doped ZnS were synthesized by chemical co-precipitation method. Analytical grade 0.4 M of zinc acetate was dissolved in 50 mL deionized water in a beaker and heated on a hot plate at 60 ºC with stirring for about 0.5 h and added PVP for controlling the nanoparticle size. After 0.5 h, an equimolar aqueous solution of sodium sulphide (0.4 M) was added dropwise into the above solution with vigorous stirring when the solution become slightly colloidal. After that the precipitated compound was removed by filtration using filter paper. The compound washed with deionized water for several times, dried overnight, crushed into fine powder and stored in a deccicator. Similar method was followed for the synthesis of cobalt doped zinc sulphide (Co:ZnS) nanoparticle by maintaining all the prerequisits and adding cobalt acetate solution in de-onized water along with $Zn(CH_3COO)_2$ and with PVP. The third compound (uncapped Co:ZnS) was prepared by following the same method but without adding PVP.

Photocatalytic activity: At different time intervals, the photocatalytic degradation of Eriochrome black T was studied using capped and uncapped Co:ZnS. At 34 ºC, Eriochrome black T was degraded in sunlight. Under sonication, in 30 mL of double distilled water, 30 mg of capped Co:ZnS nanoparticles was dispersed. Subsequently, the resulting solution was mixed with Eriochrome black T (0.0001 g/L). To achieve absorption/desorption between Eriochrome black T and the catalyst and the equilibrium, this solution was stirred at room temperature in dark for 1 h. Then, the solution was stirred with a magnetic stirrer in sunlight. At a time interval of each 20 min, the solution (3 mL) was removed from the reaction mixture to obtain the UV-visible absorption spectrum to analyze Eriochrome black T photodegradation. This process was repeated for studying other PVP uncapped Co:ZnS nanoparticles. The degradation efficiency of capped and uncapped nanoparticles was calculated as follows [29]:

$$\text{Degradation } (\%) = \frac{A_o - A_t}{A_o} \times 100 \quad (1)$$

where A_o and A_t are the initial absorbance of the sample and at the irradiation time of sample 't' of absorbance, respectively.

RESULTS AND DISCUSSION

XRD studies: Fig. 1 showed the typical powder XRD pattern of prepared capped and uncapped ZnS nanoparticles. ZnS nanoparticles showed crystalline nature with sharp peaks. Three stronger peak obtained at 28.83º, 48.71º, 56.88º indicate the crystalline structure (JCPDS. File No. 050566). In each of this patterns three reflections planes (111), (220) and (311) were observed, which indicate the cubic zinc blende structure

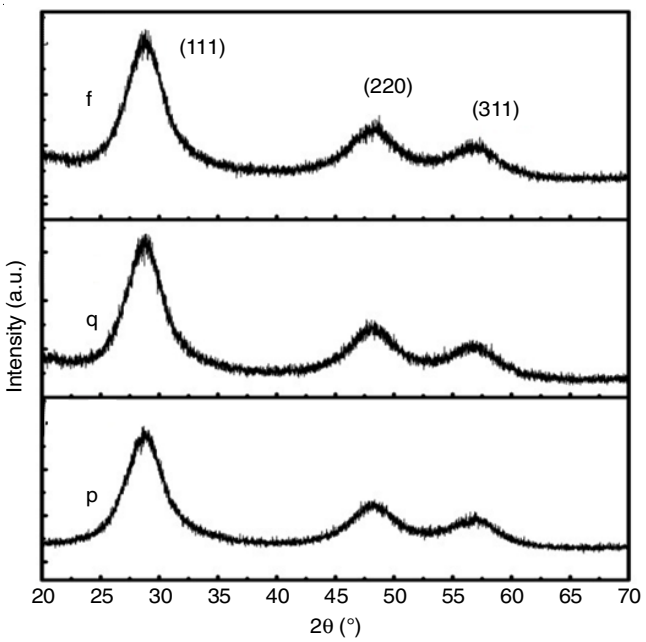

Fig. 1. XRD pattern of (p) ZnS, (q) PVP capped and (f) Uncapped Co:ZnS nanoparticles

[30]. Dopant addition causes changes in the peak intensity and position. Peak broadening indicates nanocrystal formation in the samples, and broadening increases with the substitution of Zn^{2+} ions by Co^{2+} ions. The studied sample was fabricated at room temperature (28 ºC). The broad diffraction peaks were obtained due to the small particle effect. At a low angle, peak broadening is critical for particle size calculation. The average crystalline size was calculated using Debye-Scherrer formula. The size of prepared Co-doped Zns nanoparticles substantially increased compared with that of ZnS nanoparticles through a change in the volume fraction, which depended on the dopant properties. Capped cobalt doping leads to a decrease in the average ZnS particle size.

$$D = \frac{0.94\lambda}{\beta\cos\theta} \quad (2)$$

where, D is the particle size, λ is the wavelength of X-rays (1.5405 Å), β is the full width at half maximum after correcting the instrument peak broadening (β expressed in radians) and θ is the Bragg's angle. Inter-planar spacing d (Å) and average grain size obtained by XRD studies for ZnS:Co nanocrystallites. The average size of nanoparticles was 2.27 (Å). With impurity addition, the XRD peak slightly shifted. The crystalline sizes of capped Co:ZnS nanoparticles, uncapped Co:ZnS and pure ZnS were 2.28, 2.3, and 2.25 Å, respectively. The capping agent leads to a decrease in nanoparticle crystallinity. Moreover, capped Co:ZnS provides excellent photodegradation and crystalline size compared with uncapped Co:ZnS nanoparticles.

FTIR studies: Absorption bands were recorded in the rage 4500-400 cm^{-1} and is shown in Fig. 2.The broad band appears at 3448 cm^{-1} is attributed to O-H stretching mode of moisture absorbed on the surface of the nanoparticles. The most striking evidence from FTIR spectrum of PVP stabilized Co:ZnS absorption peak 1650 cm^{-1}, which represent the

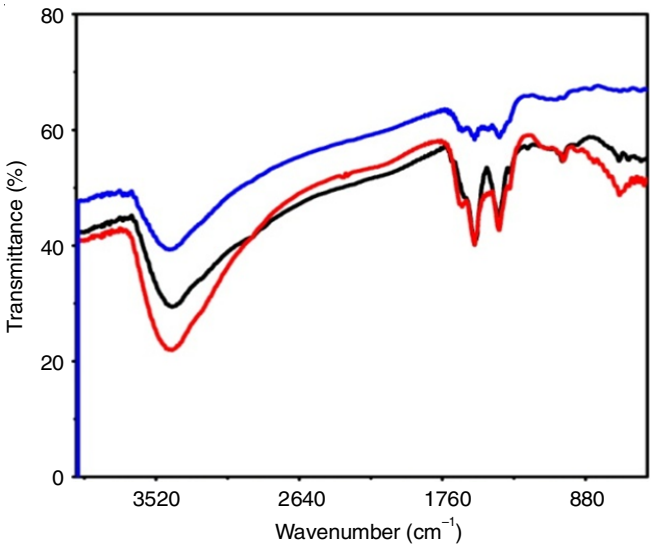

Fig. 2. FTIR spectra of pure ZnS, capped and uncapped Co:ZnS nanoparticles

functional group C=O present in PVP. The strong absorption band near 656 and 1006 cm^{-1} are assigned to Zn-S vibrations [31]. Capped and uncapped Co:ZnS samples show a blue shifts in the position of the absorption bands.

UV-visible studies: For uncapped ZnS nanoparticles, capped ZnS nanoparticles and pure ZnS, strong absorption peaks were observed at 334, 300 and 292 nm, respectively. The sharp decrease in absorption was caused by the narrow size distribution of nanoparticles. After cobalt metal doping, the absorption edge exhibited a blue shift in the nanoparticle spectra (Fig. 3). The absorption edge slightly shifted because of the quantum confinement effect generated by the nucleation rate that increased with doping leading to formation of nanoparticles. Absorption spectrum of semiconductors plays an important role to investigate their band gap energy, From the absorption spectra, the value of the band gap obtained for ZnS was 3.8 eV, the band gap for capped and uncapped Co:ZnS nanoparticles were 4.1 eV and 4.2 eV, respectively. The band gap increases with the decrease in the particles size. The increase

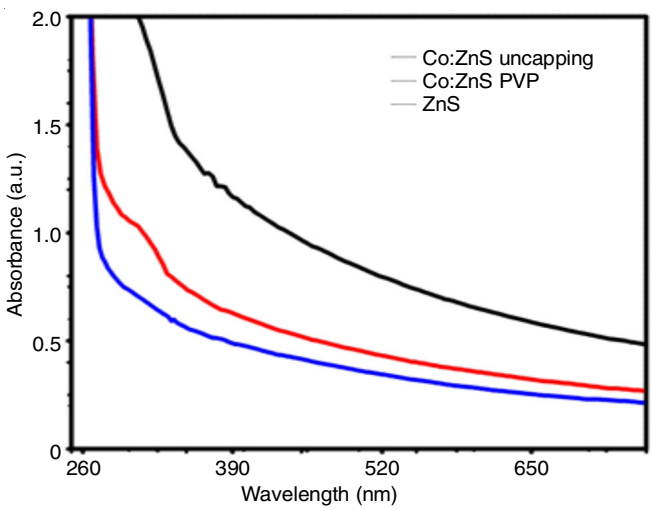

Fig. 3. UV-visible absorption spectra of the pure ZnS, PVP capped and uncapped Co:ZnS nanoparticles

in band gap with reduced particle size, indicate the strong quantum confinement effect, which were higher than the bulk value.

Photoluminescence activity: Fig. 4a-b shows the photoluminescence (PL) spectra of pure ZnS, capped and uncapped Co:ZnS nanoparticles with a excitation wavelength 325 nm and the photoluminescence emission spectra of the synthesized nanoparticles were recorded at room temperature. In photoluminescence spectra, pure ZnS nanoparticles exhibited only blue luminescence emission peaks at 410 and 438 nm related to the point defect of ZnS nanoparticles. These peaks appeared in the blue region due to recombination of electrons of the valence band and sulphur vacancy related donors [32,33]. The PL spectrum of capped and uncapped showed orange shift compared to the peak position spectrum of Co:ZnS . The red shift of photoluminescence emission for Co:ZnS may be due to the emission of photon from a wide band gap of ZnS and then recombination was observed at 649 nm. In addition, this photoluminescence emission showed a strong blue shift when compared with ZnS, indicate a successful formation of Co:ZnS nanoparticles. It is noticed that the photoluminescence intensity of ZnS nanoparticle significantly increases, as cobalt ion are doped. This intensity of blue emission decreases and orange emission comes up, since, the energy transferred from ZnS host towards dopant centers is very efficient. The synthesized Co:ZnS nanoparticles shows efficient emission of red band with peak at 649 nm with blue emission suppressed.

After the addition of the capping agent to cobalt, the luminescence intensity enhanced considerably. The intensity decreased when Co:ZnS nanoparticles were uncapped in the doped samples, which could be correlated with the XRD data. With an increase in the dopant concentration, the full-width-at-half-maximum intensity of XRD peaks increased (Fig. 1), revealed that the particle size decreased with the capping agent addition. With the particle size decrease, surface defects enhanced, which resulted in the increased PL intensity with capping agent addition. Thus, Co^{2+} acts as the sensitizing agent and improves radiative recombination. Therefore, the fluorescence efficiency of the undoped samples is lower than that of the doped samples [34].

Photocatalytic activity: The photocatalytic behaviour of uncapped and capped Co:ZnS nanoparticles towards Eriochrome black T degradation was studied with visible light irradiation. Without a catalyst, no detectable Eriochrome black T degradation occurred in sunlight, indicating that degradation only occurred because of the catalyst. PVP-capped Co:ZnS nanoparticles exhibited a higher degradation efficiency than the uncapped Co:ZnS nanoparticles.

Fig. 5 showed the photocatalytic absorption spectra of Erichrome Black T dye solution having, PVP uncapped and capped Co:ZnS nanoparticles, which have been taken at different intervals of times after exposing the solution in natural solar light. The intensity of main absorption band decreased and the solution become colourless due to the degradation of Erichrome Black T dye. The colour intensity decreases as the contact time increases. The time duration of degradation was 160 min. Fig. 6 represent the percentage Erichrome Black T dye degradation in the presence of capped and uncapped Co:ZnS nanoparticles. The time of degradation of dye have become more in case of uncapped Co:ZnS when exposure to the sunlight. The PVP capped Co:ZnS showed a higher photocatalytic activity than the uncapped Co:ZnS nanoparticles. It is also noticed that the broad band at 596 nm is due to Erichrome Black T dye (Fig. 5a-b), The band intensity decreases and its shifts to lower wavelength region as the degradation confirmed. In the presence of PVP capped Co:ZnS, the percentage degradation of Erichrome Black T dye was 92% in 140 min while with uncapped Co:ZnS the time taken for degradation occurs to be 70% in 140 min.

SEM-EDX studies: The SEM and EDX images are shown in Fig. 7a-f for ZnS, capped and uncapped Co:ZnS nanoparticles. Fig. 7a illuminate that ZnS nanoparticles are getting assembled and showed like flakes and as micro/nanoparticle. The EDS image represents the presence of Zn and S elements. Once the nanoparticle doped with Co^{2+}, a spherulitic structure has been

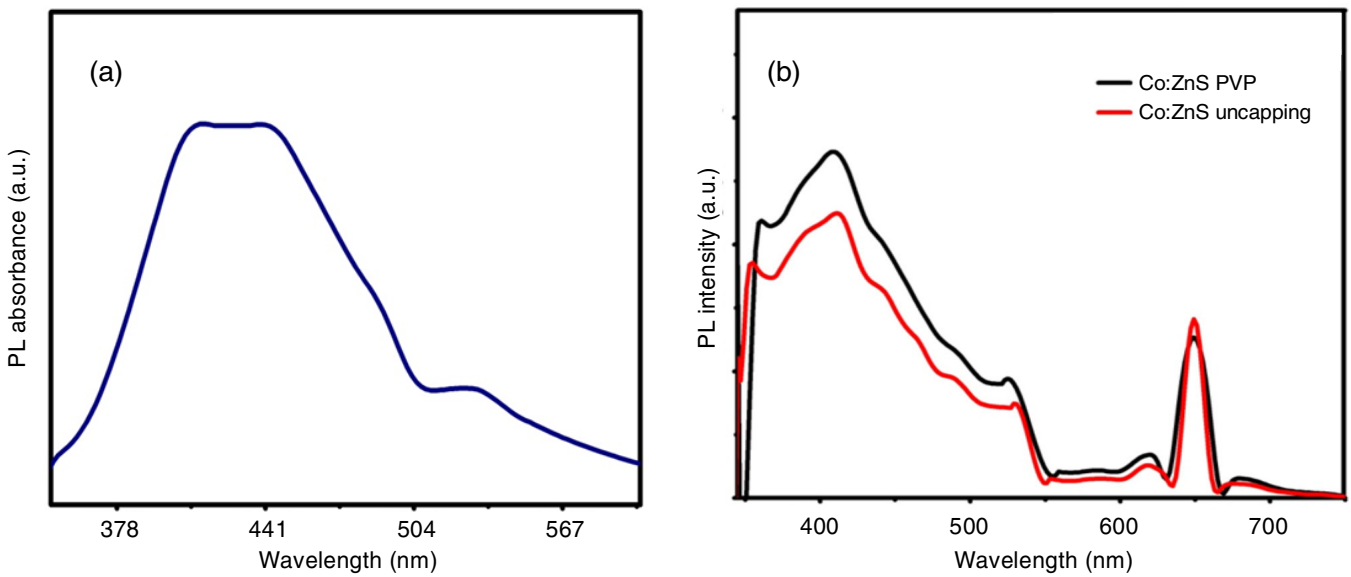

Fig. 4. Photoluminescence spectra of pure (a) ZnS, (b) capped and uncapped Co:ZnS nanoparticles

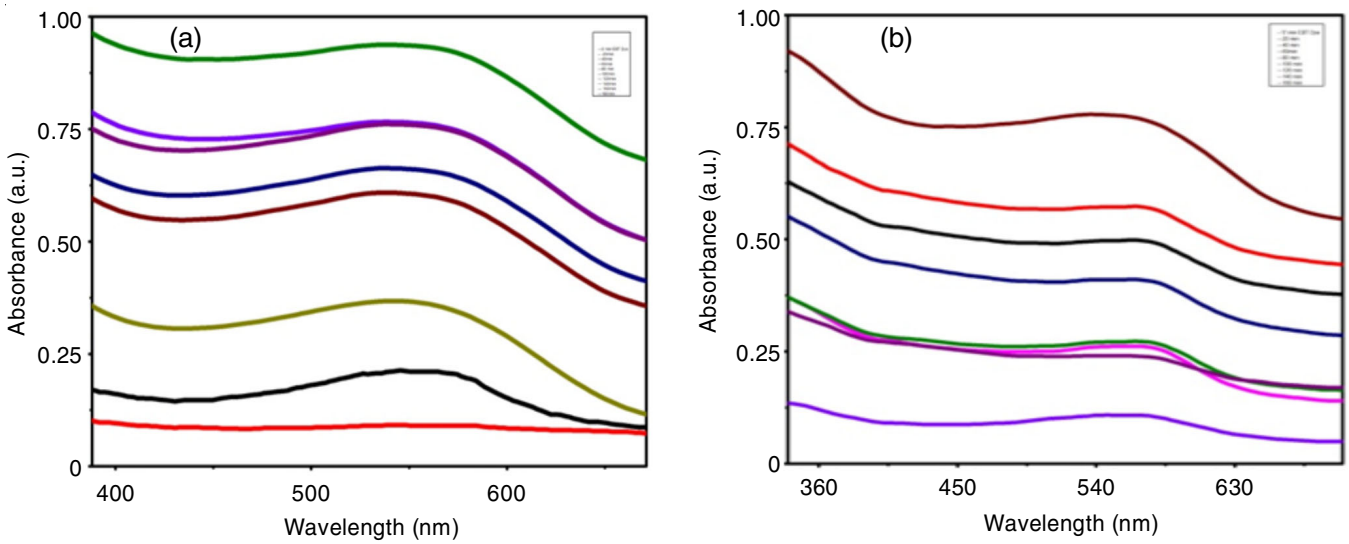

Fig. 5. Photodegradation of Erichrome black T solution at different time intervals with (a) capped and (b) uncapped Co:ZnS nanoparticles

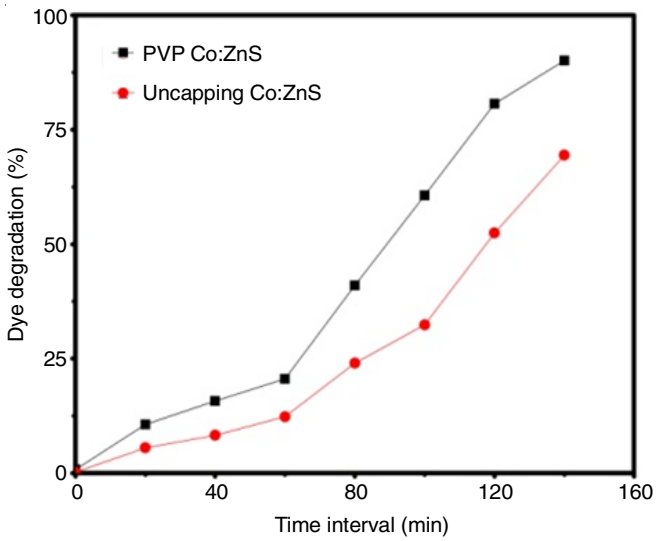

Fig. 6. Effect of time on Erichrome black T degradation in presence of capped and uncapped Co:ZnS nanoparticles

observed in SEM images of Co:ZnS nanoparticles and indicated the uniform spherical shape of the Co:ZnS nanoparticles which were arranged in a form of a cluster and a large homogeneity at the surface also observed. Fig. 7c- f represent the SEM and EDAX images of capped and uncapped nanoparticles, respectively and the EDAX of Co:ZnS nanoparticle indicates the presence of Zn, S and Co elements.

Electrochemical analyses of Co:ZnS modified electrode: By using a $K_4[Fe(CN)_6]$ (0.5 mM) redox probe in a buffer solution, the charge transfer behaviour of nanoparticle doped GCE (Co:ZnS) was studied. Fig. 8 illustrates the cyclic voltammogram (CV) for the redox couple of $[Fe(CN)_6]^{3-/4-}$ with and without the PVP capped Co:ZnS drop-coated electrode present in phosphate buffer pH 7.0 comprising $K_4[Fe(CN)_6]$ (0.5 mmol). In redox probe, for the drop coated with PVP-capped Co:ZnS electrode, a small shift in the peak current and potential intensified compared with that for bare GCE. The CV profile of nanoparticles with a large surface area for redox systems suggested that the chemisorbed surface did not completely inhibit fast electron charge transfer. This charge transfer behaves as the electron mediator between the electrolyte species and electrode. Few thin films of Co:ZnS worsen the ion immobility and trapping and inhibit the facile current flow. Co:ZnS with supported PVP-capped materials exhibits an increase in the peak current of ferrocyanide systems, indicating that PVP-capped Co:ZnS electrodes provide an easy pathway for the interaction of the buffer solution with modified electrode and promote electron transfer.

Electrochemical oxidation of dopamine (DA): To analyze the electrochemical behaviour of dopamine at the modified glassy carbon electrode, at a scan rate of 50 mV/s and modified and bare GCE, CV was acquired using a buffer solution of pH 7 which comprised different dopamine concentrations [35]. The results were recorded with the curve. The CV response of dopamine was obtained on a thin film of coated GCE under the following conditions. The applied potential was 0.35 V and dopamine (0.02 µM) was constantly added to a buffer of pH 7 with constant stirring (500 rpm) at a time interval of 40-50 s (Fig. 9). The thin film of GCE exhibited rapid improvement in CV response with dopamine addition and the signal stabilized within 3-4 s, which was important for the production of an efficient electrode. Within 3 s after dopamine addition, 97% steady-state current was attained, which revealed the efficiency and rapid detection of modified GCE for dopamine. The linear response between the dopamine concentration and CV growing step currents was good (Fig. 9a-b). This response satisfied the equation: $y = 4.3663(DA) + 5.219$. At Co:ZnS/GCE for dopamine, the slope was 4.3663 µA μM^{-1}. In 0.2-1.6 µM/L, for dopamine, the concentration was observed linearly on the electrode. GCE exhibited considerably high electrocatalytic activity for dopamine oxidation. The Co:ZnS/GCE exhibited an excellent LOD and sensitivity. For dopamine, the LOD of GCE/Co:ZnS, the modified electrode, was 0.06 µM/L. LOD was calculated using the formula: 3.3 (σ/s), where s denotes the calibration curve slope and s represents the standard deviation of the mean value of 10 dopamine additions.

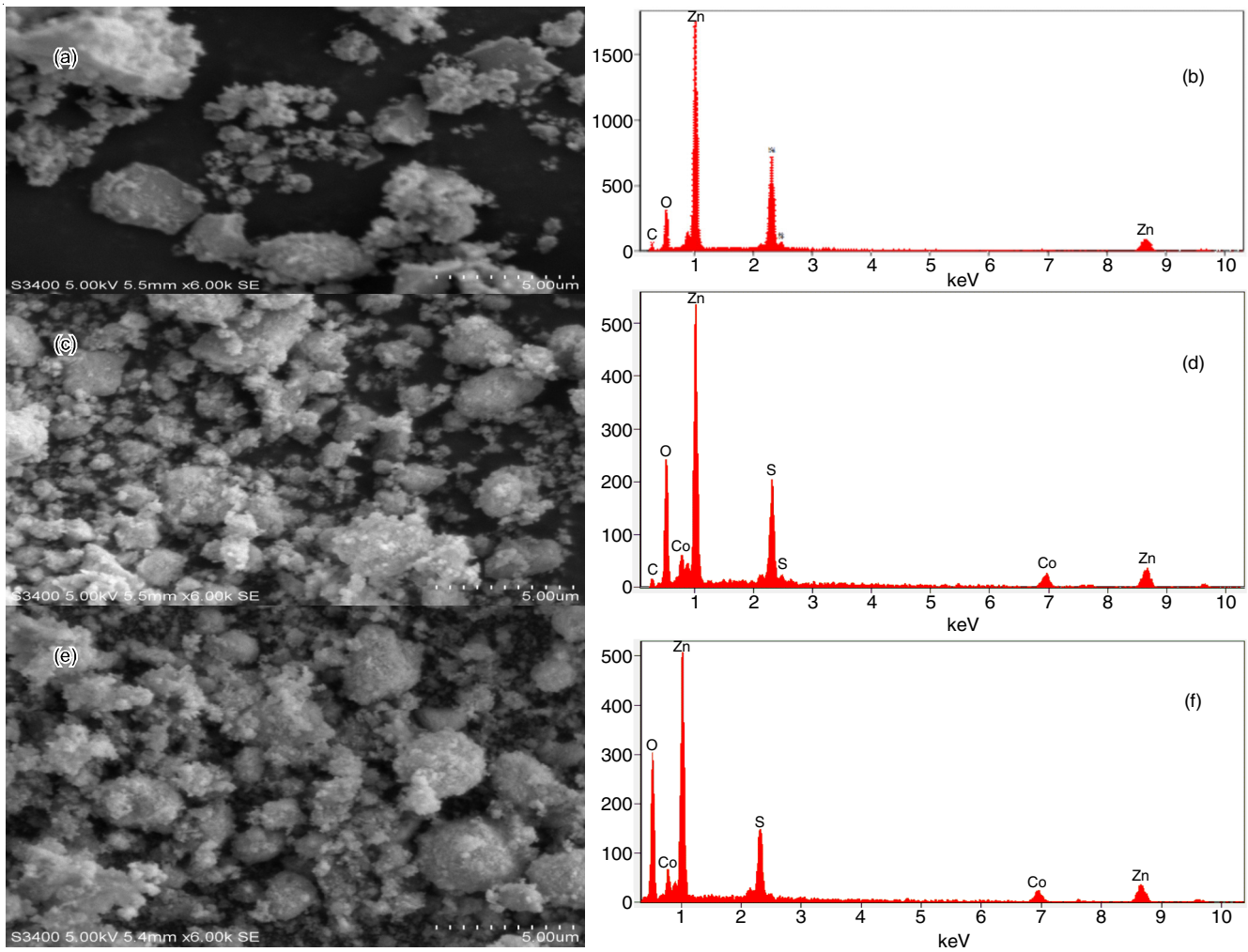

Fig. 7. SEM and EDS images of ZnS (a, b), PVP-Co: ZnS (c, d) and uncapped Co:ZnS (e, f)

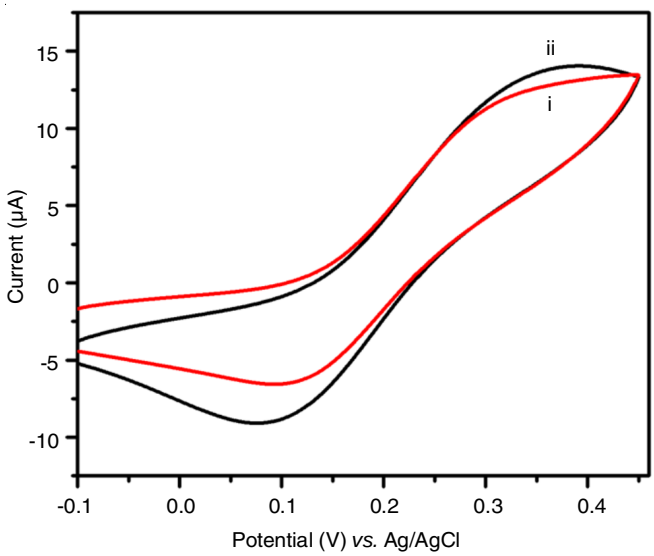

Fig. 8. Cyclic voltammograms of (i) Bare GCE (ii) Co:ZnS/GCE in 1 mM $K_4[Fe(CN)_6]$, Scan rate = 50 mV/s

Effect of scan rate: The CV were recorded for 10 µM dopamine in buffer solution pH 7 at different scan rates (Fig. 10a). The value of peak current increases as the scan rate increases from 10 to 200 mV s^{-1}. A plot of I_{pa} *versus* exhibited linear relationship indicating the diffusion controlled mass transfer process (Fig. 10b) [36].

Effect of different concentration of uric acid: Fig. 11a shows the CV response of the GCE electrode in uric acid with different concentrations. The oxidation peak currents were linear and Fig. 11b related to the uric acid concentration in the range of 0.5 to 01.01 µM with the correlation coefficient I_p = 2.454 (UA) + 2.206 (µM) (R^2 = 0.99545). The sensitivity and detection limit of the modified GC electrode was 2.2066 µA $µM^{-1}$ cm^{-2} and 0.166 µM, respectively. The reported the electrochemical determinations of uric acid using different electrodes are summarized in Table-1. The results showed that the electrode possesses a satisfactory sensitivity and low measured LOD for the detection of uric acid. The oxide peak current of uric acid displays a linear relationship with the concentration of uric acid. The corresponding equations is $I_p = (2.2065 \pm 0.43) + (2.453 \pm 0.01)$ (R^2 = 0.996) [37].

Conclusion

The pure ZnS capped and uncapped Co:ZnS nanoparticles were successfully synthesized by co-precipitation method using poly(vinyl pyrrolidone) (PVP) as capping agent. Synth-

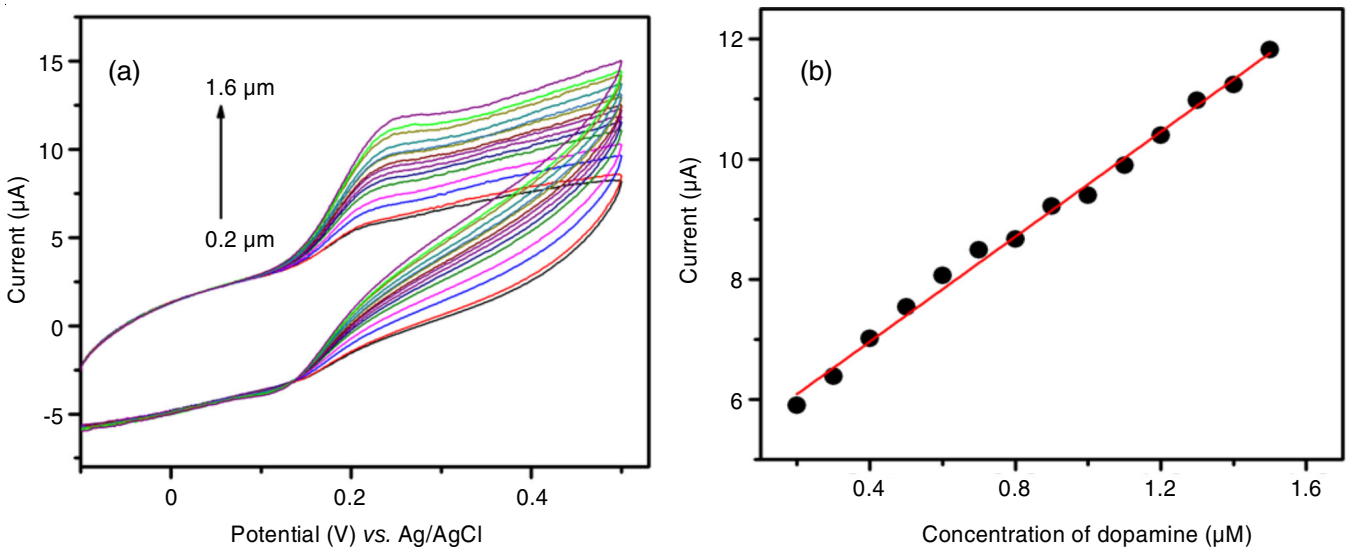

Fig. 9. (a) Cyclic voltammogram of dopamine at modified Co:ZnS/GCE at different concentration of dopamine ranging from (0.2 to 1.6 µM). And (b) Inset: calibration graph of current *vs.* concentration

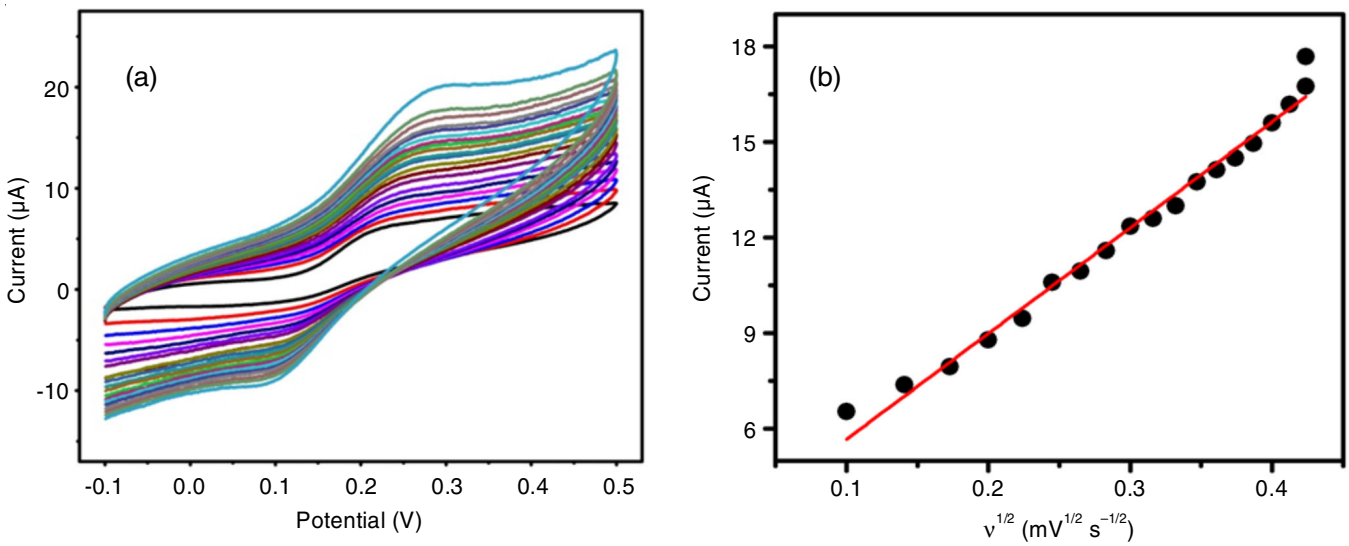

Fig. 10. (a) Cyclic voltammogram of dopamine at Co:ZnS/GCE scanning rate ranging from (10 to 200 mV s^{-1}). (b) The plot of current *vs.* $v^{1/2}$

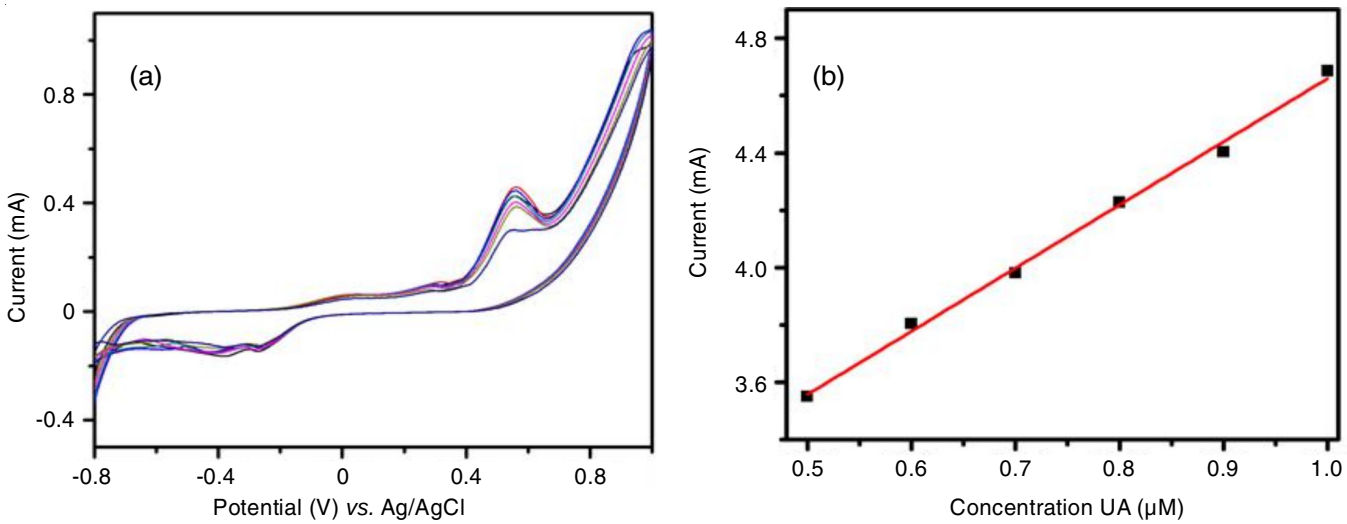

Fig. 11. CV plot of (a) modified GCE of different concentrations (0.5-01 µM) of uric acid (UA), at scan rates 50 m *vs.* and (b) Linear plot of peak current *vs.* concentration of uric acid (UA)

TABLE-1
DIFFERENT COMPOSITE MATERIALS USED FOR DETECTION OF DOPAMINE

Electrode	Detection methods	Sample	Linear range (μmol/L)	Sensitivity (μA μM^{-1})	LOD (μmol L^{-1})	Ref.
GCE/rGO-Zn(II)TPEBiPc	CV	Dopamine	0.2-10	2.173	0.0660	[38]
rGo-Co_3O_4	CV	Dopamine	0-30	0.389	0.0092	[39]
Azo-bridzed-CuPc polymer/GCE	CV	Dopamine	10-160	0.078	0.3300	[40]
$LaFeO_3$/ITO	CV	Dopamine	5-200	–	0.0060	[41]
Binuclear copper(II) modified Au	DPV	Dopamine	0.2-30	0.03	0.0800	[42]
Protocatechuic acid-Cys modified Au	CV	Dopamine	4.3-900	–	1.6000	[43]
Co(II)complex/GCE	CV	Dopamine	0.3-3.9	0.532	0.1000	[44]
CoZnS/GCE	CV	Dopamine	0.2-1.6	4.366	0.0660	Present work

esized nanoparticles were characterized by physico-chemical, spectral, photocatalytic and optical absorption studies. FTIR confirmed the formation of nanoparticles by comparing the shifts in the position of peaks of capped and uncapped Co:ZnS nanoparticles. The XRD results showed that cobalt doped ZnS nanoparticles exhibit a zinc blende structure with uniform size. Eriochrome black T photocatalytic degradation indicated that prepared PVP capped Co:ZnS nanoparticles can be employed as potential catalysts in photocatalytic degradation compared with uncapped Co:ZnS nanoparticles. Eriochrome black T degraded to >92% with PVP. Without PVP, 92% degradation occurred; however, the degradation time was relatively longer. The nanoparticle morphology indicated that the photocatalytic activity occurred on a nanoscale in sunlight. The new Co:ZnS/GCE modified glassy carbon electrode has been evaluated using Co:ZnS/GCE. The drop coated electrode offers high stability, reproducibility, high and a distinct advantage of polishing in the event of surface fouling. The synthesized Co:ZnS/GCE nanomaterial showed the enhanced results using cyclic voltammetric techniques for detection of dopamine. The Co:ZnS/GCE modified GCE shows verygood results such as high sensitivity, LOD (0.06 μM) and long linear range value (0.2 to 1.6 μM), stability and antifouling properties. The intensity of photoluminescence emission was observed to decrease with addition of cobalt doped in ZnS.

ACKNOWLEDGEMENTS

The authors are thankful to UGST, K-FIST-L1, Manipal Institution of Technology, Manipal and University of Mysore, Mysuru, India for providing the spectral data.

CONFLICT OF INTEREST

The authors declare that there is no conflict of interests regarding the publication of this article.

REFERENCES

1. K.S. Jithendra Kumar, G. Krishnamurthy, B.E. Kumara Swamy, N.D. Shashi Kumar, S. Naik, B.S. Krishna and N. Naik, *Appl. Organomet. Chem.*, **31**, e3549 (2016); https//doi.org/10.1002/aoc.3549
2. K.R. Sumadevi and G. Krishnamurthy, P. Walmiki, R.S. Priya Rani, S. Naik, H.S. Bhojya Naik and N. Naik, *Emergent Mater.*, **4**, 447 (2021); https://doi.org/10.1007/s42247-020-00153-7
3. K.S. Jithendra Kumara, G. Krishnamurthy, N. Sunil Kumar, N. Naik and T.M. Praveen, *J. Magn. Magn. Mater.*, **451**, 808 (2018); https://doi.org/10.1016/j.jmmm.2017.10.125
4. S. Li, M.M. Lin, M.S. Toprak, D.K. Kim and M. Muhammed, *Nano Rev.*, **1**, 5214 (2010); https://doi.org/10.3402/nano.v1i0.5214
5. W.I. Choi, J.Y. Kim, S.U. Heo, Y.Y. Jeong, Y.H. Kim and G. Tae, *J. Control. Rel.*, **162**, 267 (2012); https://doi.org/10.1016/j.jconrel.2012.07.020
6. M.J. Hajipour, K.M. Fromm, A.A. Ashkarran, D.J. de Aberasturi, I.R. Larramendi, T. Rojo, V. Serpooshan, W.J. Parak and M. Mahmoudi, *Trends Biotechnol.*, **30**, 499 (2012); https://doi.org/10.1016/j.tibtech.2012.06.004
7. N.R. Agarwal, F. Neri, S. Trusso, A. Lucotti and P.M. Ossi, *Appl. Surf. Sci.*, **258**, 9148 (2012); https://doi.org/10.1016/j.apsusc.2011.12.030
8. Y. Dong and S.S. Feng, *Int. J. Pharm.*, **342**, 208 (2007); https://doi.org/10.1016/j.ijpharm.2007.04.031
9. W. Tungittiplakorn, L.W. Lion, C. Cohen and J.-Y. Kim, *Environ. Sci. Technol.*, **38**, 1605 (2004); https://doi.org/10.1021/es0348997
10. A.V. Kachynski, A.N. Kuzmin, M.M. Nyk, I. Roy and P.N. Prasad, *J. Phys. Chem.*, **112**, 10721 (2018); https://doi.org/10.1021/jp801684j
11. Z. Zhou, C. Zhang, Q. Qian, J. Ma, P. Huang, X. zhang, L. Pan, G. Gao, H. Fu, S. Fu, H. Song, X. Zhi, J. Ni and D. Cui, *J. Nanobiotechnology*, **11**, 17 (2013); https://doi.org/10.1186/1477-3155-11-17
12. E.C. Cho, C. Glaus, J. Chen, M.J. Welch and Y. Xia, *Trends Mol. Med.*, **16**, 561 (2010); https://doi.org/10.1016/j.molmed.2010.09.004
13. X. Huang, P.K. Jain, I.H. El-Sayed and M.A. El-Sayed, *Lasers Med. Sci.*, **23**, 217 (2008); https://doi.org/10.1007/s10103-007-0470-x
14. T.G. Smijs and S. Pavel, *Nanotechnol. Sci. Appl.*, **4**, 95 (2011); https://doi.org/10.2147/NSA.S19419
15. G.J. Nohynek, E.K. Dufour and M.S. Roberts, *Skin Pharmacol. Physiol.*, **21**, 136 (2008); https://doi.org/10.1159/000131078
16. J.J. Wu and S.C. Liu, *Adv. Mater.*, **14**, 215 (2002); https://doi.org/10.1002/1521-4095(20020205)14:3<215::AID-ADMA215>3.0.CO;2-J
17. J. Zhong, J. Li, Z. Xiao, W. Hu, X. Zhou and X. Zheng, *Mater. Lett.*, **91**, 301 (2013); https://doi.org/10.1016/j.matlet.2012.10.040
18. K.M. Parida and S. Parija, *Sol. Energy*, **80**, 1048 (2006); https://doi.org/10.1016/j.solener.2005.04.025
19. M. Farbod and M. Kajbafvala, *Powder Technol.*, **239**, 434 (2013); https://doi.org/10.1016/j.powtec.2013.02.027
20. R.K. Upadhyay, M. Sharma, D.K. Singh, S.S. Amritphale and N. Chandra, *Sep. Purif. Technol.*, **88**, 39 (2012); https://doi.org/10.1016/j.seppur.2011.11.040
21. P. Chandran, S. Netha, A. Ravindran and S.S. Khan, *J. Colloid. Surf. B*, **122**, 611 (2014); https://doi.org/10.1016/j.colsurfb.2014.07.039
22. P. Chandran, S. Netha and S.S. Khan, *J. Photochem. Photobiol. B*, **138**, 155 (2014); https://doi.org/10.1016/j.jphotobiol.2014.05.013

23. P. Yang, M. Lü, D. Xü, D. Yuan, C. Song and G. Zhou, *J. Phys. Chem. Solids*, **62**, 1181 (2001); https://doi.org/10.1016/S0022-3697(00)00287-0
24. H. Hu and W. Zhang, *Opt. Mater.*, **28**, 536 (2006); https://doi.org/10.1016/j.optmat.2005.03.015
25. W.Q. Peng, G.W. Cong, S.C. Qu and Z.G. Wang, *Opt. Mater.*, **29**, 313 (2006); https://doi.org/10.1016/j.optmat.2005.10.003
26. N. Murase, R. Jagannathan, Y. Kanematsu, M. Watanabe, A. Kurita, K. Hirata, T. Yazawa and T. Kushida, *J. Phys. Chem. B*, **103**, 754 (1999); https://doi.org/10.1021/jp9828179
27. S. Yanagida, M. Yoshiya, T. Shiragami, C. Pac, H. Mori and H. Fujita, *J. Phys. Chem.*, **94**, 3104 (1990); https://doi.org/10.1021/j100370a066
28. L. Liu, L. Yang, Y. Pu, D. Xiao and J. Zhu, *Mater. Lett.*, **66**, 121 (2012); https://doi.org/10.1016/j.matlet.2011.08.025
29. S. Sambasivam, D.P. Joseph, J.G. Lin and C. Venkateswaran, *J. Solid State Chem.*, **182**, 2598 (2009); https://doi.org/10.1016/j.jssc.2009.07.015
30. S. Muruganandam, G. Anbalagan and G. Murugadoss, *Optik*, **131**, 826 (2017); https://doi.org/10.1016/j.ijleo.2016.12.001
31. S. Lee, S. Song, D. Kim, J. Lee, S. Kim, I.Y. Park and Y.D. Choi, *Mater. Lett.*, **58**, 342 (2004); https://doi.org/10.1016/S0167-577X(03)00483-X
32. W.Q. Peng, G.W. Cong, S.C. Quand Z.G. Wang, *Opt. Mater.*, **29**, 313 (2006); https://doi.org/10.1016/j.optmat.2005.10.003
33. N. Shanmugam, S. Cholan, G. Viruthagiri, R. Gobi and N. Kannadasan, *Appl. Nanosci.*, **4**, 359 (2014); https://doi.org/10.1007/s13204-013-0217-x
34. N.V. Desai, I.A. Shaikh, K.G. Rawal and D.V. Shah, *AIP Conf. Proc.*, **1953**, 030149 (2018); https://doi.org/10.1063/1.5032484
35. H.Y. Yue, P.F. Wu, S. Huang, X. Gao, S.S. Song, W.Q. Wang and X.R. Guo, *Microchem. J.*, **149**, 103977 (2019); https://doi.org/10.1016/j.microc.2019.103977
36. N. Arif, S. Gul, M. Sohail, S. Rizwan and M. Iqbal, *Ceram. Int.*, **47**, 2388 (2021); https://doi.org/10.1016/j.ceramint.2020.09.081
37. Y.J. Yang, *Sens. Actuators*, **22**, 750 (2015); https://doi.org/10.1016/j.snb.2015.06.150
38. M. Pari, K.R.V. Reddy, Fasiulla and K.B. Chandrakala, *Sens. Actuators A Phys.*, **316**, 112377 (2020); https://doi.org/10.1016/j.sna.2020.112377
39. A. Numan, M.M. Shahid, F.S. Omar, K. Ramesh and S. Ramesh, *Sens. Actuators B Chem.*, **238**, 1043 (2017); https://doi.org/10.1016/j.snb.2016.07.111
40. M. Pari, Mounesh, J.B. Sanna and K.R. Venugopala Reddy, *Anal. Bioanal. Electrochem,*, **11**, 460 (2019).
41. Z.T. Althagafi, J.T. Althakafy, B.A. Al-Jahdaly and M.I. Awad, *J. Sensors*, **2020**, 8873930 (2020); https://doi.org/10.1155/2020/8873930.
42. Y. Kumar, S. Pramanik and D.K. Das, *Biointerf. Res. Appl. Chem.*, **10**, 6182 (2020); https://doi.org/10.33263/BRIAC105.61826188
43. G. Jiang, X. Gu, G. Jiang, T. Chen, W. Zhan and S. Tian, *Sens. Actuators B Chem.*, **209**, 122 (2015); https://doi.org/10.1016/j.snb.2014.11.109
44. N. Sunil Kumar, G. Krishnamurthy, M. Somegowda, M. Pari, T.R. Ravikumar Naik, K.S. Jithedra Kumara, S. Naik, S. Kandagalla and N. Naik, *J. Mol. Struct.*, **1220**, 128586 (2020); https://doi.org/10.1016/j.molstruc.2020.128586